J Appl Electrochem (2014) 44:115–121
DOI 10.1007/s10800-013-0613-7

RESEARCH ARTICLE

Zn–Ni/nano-TiO_2 composite electrodeposits: surface modifications and protective properties

Olfa Hammami · Leila Dhouibi · Patrice Berçot · El Mustafa Rezrazi

Received: 12 February 2013 / Accepted: 10 August 2013 / Published online: 4 September 2013

Abstract Zn–Ni composite coatings were obtained by electrochemical co-deposition of TiO_2 nano-particles (mean diameter 21 nm). Zn–Ni alloy coating was also produced under the same experimental conditions for comparison. The surface morphology, crystallographic structure, and the grain size of the deposits were investigated, along with the percentage of the embedded nano-particles in Zn–Ni matrix, as a function of concentration of TiO_2 nano-particles in the bath. As the titania incorporation percentage is increased, a grain refinement in the nanometer region was revealed followed enhanced microhardness values and an improvement of the content of the nickel in the alloy. Annealing of all coatings at 200 °C revealed the crystallization of the matrix accompanied by a decrease of microhardness followed by stability for 24 h. The corrosion behavior of Zn–Ni/nano-TiO_2 composite coatings with various amount of particle content was mainly studied by electrochemical impedance spectroscopy in 3 % NaCl. It was seen that Zn–Ni/nano-TiO_2 composite coatings exhibited higher corrosion resistances comparing to Zn–Ni alloy coating and corrosion protection improved with increasing nano-TiO_2 in coatings.

Keywords Zn–Ni alloy · Composite coatings · Thermal treatment · Corrosion resistance · TiO_2 nano-particles

O. Hammami (✉) · L. Dhouibi
Unit of Research « COPROMET » ENIT,
BP 37, 1002 Belvedere, Tunisia
e-mail: yefate7@yahoo.fr

O. Hammami · P. Berçot · E. M. Rezrazi
Institut UTINAM, CNRS UMR 6213, Équipe Sonochimie et Réactivité des Surfaces, Université de Franche-Comté,
16 route de Gray, 25030 Besançon Cedex, France

1 Introduction

The need for coatings with improved resistance to highly aggressive environments is high as a result of a growing demand for extended safe service life of industrial objects. One of the ways to increase the corrosion resistance of zinc coatings consists in alloying with Fe, Co, Ni. It was reported that Zn coatings containing up to 12 % Ni provide cathodic protection to steel, exhibiting significantly higher corrosion resistance than pure zinc [1]. An alternate process for enhancing the corrosion resistance of zinc coatings on steel consists in zinc composite coating on its surface by electrolysis of plating solutions, in which sub-micron or nano size particles (i.e., TiO_2, SiO_2, Al_2O_3 etc.) are suspended [2–5]. Their incorporation in the coating Ni–Zn refines the crystal size and enhances corrosion resistance, microhardness, and wear resistance property [6–8]. Metal matrix composite coatings containing TiO_2 particles exhibited interesting photo-electrochemical and photo-catalytical behavior [7, 9] accompanied by improved mechanical properties [10, 11]. Especially, research related to Ni–TiO_2 composite coatings had demonstrated that the co-deposition percentage of nano-titania particles was difficult to be controlled quantitatively, because the particles were frequently agglomerated in the metal matrix, as well as in the electrolyte [12, 13] due to their significant high surface energy. Given that TiO_2 particles seemed to incorporate in a limited extend compare to other ceramic particles, like SiC particles in example [14], the major challenges were the enhancement of particles incorporation accompanied by their uniform distribution in the deposit. It should be mentioned that the highest amount of nano-titania embedded particles did not exceed ~3.5 vol% [15] in the presence of organic additives by using Watts type bath.

Taking into consideration all the above-mentioned data, we had conducted a comprehensive study in an extended area. In fact, we studied the influence of particles with concentration of 5 and 10 g L^{-1} on the surface morphology, crystal size, and the structure of the Zn–Ni alloy coatings.

2 Experimental

2.1 Electroplating process

The chemical compositions of the basic non-agitated electrolyte of Zn–Ni alloys deposition is given in Table 1 [16]. All experiments were carried out in duplicated and the ability to reproduce these measurements was found satisfactory.

Galvanostatic measurements were performed on steel rod cathode which was placed in a PTFE mount for obtaining cross-sectional area of 0.2 cm^2 in contact with solution. The deposition was done on steel (STUB 100CR6) substrates. The chemical composition of STUB 100CR6 steel was 0.95 % C, 0.2 %, Mn 0.15 % Si and 0.015 % S (wt%). Initially, the steel samples were mechanically polished with successively finer grades of emery paper. They were then washed in de-ionized water. This procedure was repeated until a clear and smooth surface was obtained. To obtain fixed hydrodynamic conditions, the Zn–Ni coatings were deposited on a rotating disc electrode (RDE) with a constant rotation velocity of 1,000 rpm. The deposition experiments were performed at a current density of 25 mA cm^2 and the plating time was 15 min. The TiO_2 powder (AEROXIDE p25) with a mean diameter of 21 nm was used as received without any pretreatment.

Before electrodeposition, the nano-particles were dispersed in the bath by ultrasonic wave for 30 min. Particles with concentration of 5 g L^{-1} were maintained in an electrolytic bath in suspension by continuous magnetic stirring of 200 rpm for at least 24 h before deposition.

Table 1 Solution composition and conditions for alloy plating [16]

Electrolyte ingredients	Concentration (g L^{-1})	Plating parameters	$R_1 = [Zn^{2+}]/[Ni^{2+}]$
$ZnSO_4 \cdot 7H_2O$	57.5	pH = 2.5	1.1
$NiSO_4 \cdot 6H_2O$	52.5	temperature (°C) : 30 ± 0.5	
H_3BO_3	9.3		
Na_2SO_4	56.8		
H_2SO_4	0.53		

2.2 Electrochemical measurements

For electrochemical measurements the coated samples were exposed to 3 % NaCl solution. These studies were performed respectively with potentiostat PGP 201 and interface Solarton SI 1287/SI 1250 in a thermostatic three-electrode cell. The working electrode was a coated sample, the counter electrode was platinum with an area of 1 cm^2 and the reference electrode was saturated calomel SCE ($Hg/Hg_2Cl_2/KCl$ satured). The impedance data were obtained at the open-circuit potential and the measurements were carried out over a frequency range of 65 kHz to 10 mHz using an amplitude of sinusoidal voltage (10 mV).

2.3 Characterization studies

An X-ray diffraction investigation of Zn–Ni electrodeposits was carried out using an X-ray diffractometer D8 (Advance Bruker) equipped with a copper anode generating Ni-filtered CuKα radiation (l = 1.5405 Å, 45 kV, 40 mA). The quantity of Zn and Ni in the coatings, thicknesses, and optical surface images of coatings was determined by the means of Fiscerscope X-ray XDAL fluorescence. Surface morphology of the deposits was followed with electron microscope at 15 kV. Measurements of the Vickers microhardness (HV) of deposits were performed in the surface by using a HMV-M3 SHIMADZU Microhardness tester under 25–100 g load for 10 s and the corresponding final values were determined as the average of five measurements.

Crystallite sizes of the coatings were calculated from the X-ray peak broadening of the (330) diffraction peak using Scherrer's formula [Eq. (1)] [17];

$$D = K\lambda/(\beta\cos\theta) \quad (1)$$

where K is the Scherrer factor ≈ 1, D is the crystallite size, λ is the incident radiation wavelength, β is the integral breadth of the structurally broadened profile, and θ is the angular position.

3 Results and discussion

3.1 Nano-titania particles codeposition

Hydrophilic particles of TiO_2 interacted with the electrolyte and therefore chemical and physical adsorption of electrolyte ions onto the particle occurred. This adsorption and the initial particle surface composition determined the particle surface charge [18]. By observing the movement of particles under the influence of an electric field in the airframe microelectrophoresis "Rank Brothers II", we could determine the effective charge of particles and

calculated the electrophoretic mobility of the particle and its corresponding zeta potential. We noted positively charged particles of TiO_2. This may lead to co-deposition at the negatively charged cathode [19]. The absolute value of the zeta potential is a very important factor for the degree of particles incorporation and the stability of the electroplating solution [20]. In pH 5.9, the results revealed a value of zeta potential equal to 15 mV lower than 30 mV, showing that in the electroplating solution, conglobation trend among nano-particles increased and the dispersibility of the electroplating solution was weakened [21].

3.2 Compositional analysis and morphology

From the evaluation of the XRF results (Table 2), it was found that as the concentration of TiO_2 nano-particles in the electrolyte increased, the percentage of TiO_2 nano-particles occluded in the electrodeposit was also increased. Banovic et al. [21], as well as Chen et al. [22] proposed that increasing the number of effective collisions between the oxide particles and the cathode surface per unit volume of deposited matrix would increase the amount incorporated into the coating. According to them, this could be accomplished by increasing the number of particles suspended in the electrolyte.

The XRF analysis revealed about a double percentage of Ni in Zn–Ni alloy composite elaborated with 10 g L^{-1} TiO_2, in comparison with the alloy electroplated without loading the plating bath with nano-particles. In fact, it has been shown that the content of Ni^{2+} (aq) adsorbed on the oxide particles is greater than that of Zn^{2+} (aq) [23]. The ratio of the less noble metal Zn to the more noble metal Ni in the deposit (R_2) was larger than in the bath (R_1). This phenornenon is known as ''anomalous co-deposition,'' fully described by Brenner [24].

Figure 1 showed the SEM micrographies of Zn–Ni alloy composites. The surface morphology of Zn–Ni alloy showed branched acicular crystallite structure (Fig. 1a). The incorporation of nano-TiO_2 transformed the acicular structure to nodular. In Fig. 1b, it could be observed the presence of large agglomeration of the particles and cracks all over the surface. However, Fig. 1c showed different morphology which was fully compacted with refined grains. It seemed that the incorporation of the titania nano-particles took place between the grains in cavities as denoted in Fig. 1d. As the concentration of TiO_2 nano-particles in the electrolyte increased, the nano-particles plugged the cracks observed in the surface of Zn–Ni composite elaborated with 5 g L^{-1} TiO_2.

3.3 Phase structure

XRD studies confirmed such changes in the phase composition of the alloy. Figure 2 showed the XRD patterns for the plated Zn–Ni alloy coatings. The diffraction lines of η-(or may pure zinc), γ-Ni_5Zn_{21}, and Fe phases were observed. The diffraction peaks of TiO_2 powder were not obvious in the diffractograms of composites due to the lower content of TiO_2 embedded in the coatings. The results revealed that the η-phase quantity was very low, while the γ-phase is predominantly observed, particularly in the composite elaborated with 10 g L^{-1} nano-TiO_2. We could explain this evolution by the fact that the quantity of Zn in these deposits decreased. The Ni-content of Zn–Ni alloy deposits plays a major role in controlling the phases present and the grain size [25].

Furthermore, changes in the crystallographic structure were provoked probably by the proton adsorption on the titania particle surfaces according to Eq. (2), which inhibits the formation of H_{ads} at the cathode/catholyte interface that impose the mode of matrix growth.

$$-\mathrm{MOH} + \mathrm{H^+} \rightarrow -\mathrm{MOH_2^{\rightarrow}} - \mathrm{M^+} + \mathrm{H_2O} \qquad (2)$$

Additionally, the adsorption of H^+ on the titania particles provoked a local alkanisation of the cathode/elctrolyte interface produced by the partially hydroxylated layer around the particles as denoted in Eq. (2). Such situation indicated that hydrogen evolution is restrained to some extent. The comparison of optical surface images of Zn–Ni alloy coating and Zn–Ni alloy composite elaborated with 10 g L^{-1} nano-TiO_2 (Fig. 3) confirmed the obtained results. The composite surface looked more homogenous with reduction of asperities related to hydrogen evolution.

3.4 Microhardness and thermal stability of deposits

HV values of Zn–Ni alloy deposits were shown in Fig. 4. The evolution of coatings hardness showed an increase

Table 2 Composition analysis and thicknesses of Zn–Ni deposits

Coating systems	Thicknesses (±0.1 μm)	Ti (±0.2 wt%)	Ni (±0.2 wt%)	Zn (±0.2 wt%)	R_2 = Zn/Ni
Zn–Ni alloy coating	8	0	6.3	93.7	14.8
Zn–Ni composite (with 5 g L^{-1} TiO_2)	8.5	0.68	10.7	88.6	8.2
Zn–Ni composite (with 10 g L^{-1} TiO_2)	8.7	1.35	12.5	86.1	6.8

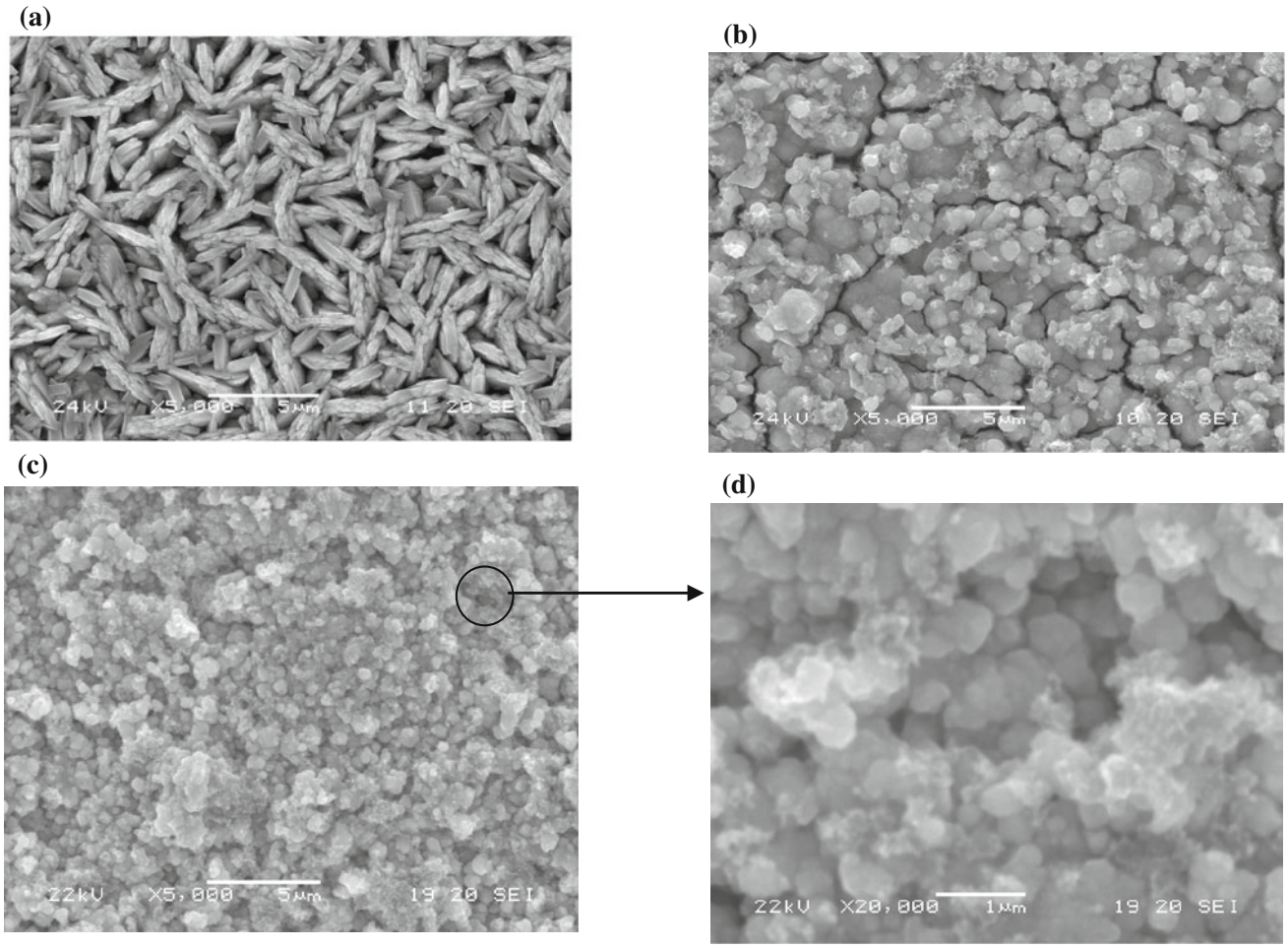

Fig. 1 SEM micrographs of the surfaces of: **a** Zn–Ni alloy coating **b** Zn–Ni alloy composite (with 5 g L^{-1} nano-TiO_2), **c**, **d** Zn–Ni alloy composites (with 10 g L^{-1} nano-TiO_2) and **d** enlargement (×20,000) of Fig. 1c

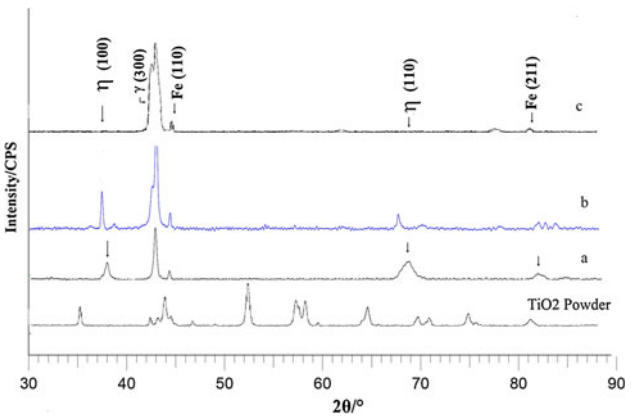

Fig. 2 X-ray diffractograms for TiO_2 powder, Zn–Ni alloy coating (*a*) and Zn–Ni alloy composites elaborated with: *b* 5 g L^{-1} nano-TiO_2 and *c* 10 g L^{-1} nano-TiO_2

from about 140 HV for Zn–Ni alloy to about 380 HV for composite coating prepared with 10 g L^{-1} nano-TiO_2. We could conclude that the microhardness was affected by the incorporation of this type of nano-particles into deposits. In turn, crystallite size is an important variable affecting the hardness value [26]. In fact, smaller crystallite size implies a greater number of grain boundaries that impede dislocation motion, and then creates harder materials. Studies concerning the incorporation of TiO_2 nano-particles had shown that the dispersed nano-particles either increase the nucleation [27] or restrain the crystal size rather by inhibiting crystal growth than by providing new nucleation surfaces [13].

The thermal stability of Zn–Ni alloy electrodeposits is important to their general evaluation for future applications, particularly in applications where the coatings are expected to perform at elevated temperature such as on some automotive parts. In this study, in order to evaluate the stability of the deposits, we followed the microhardness evolution of deposits treated at 200 °C continuously for 30 min, 2 and 24 h (Fig. 4a).

After annealing at 200 °C, deposits revealed reduced hardness values after 30 min of thermal treatment, whereas

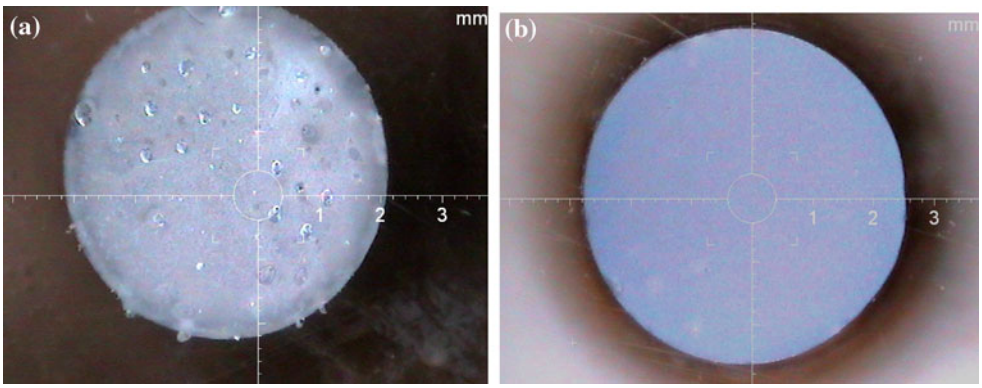

Fig. 3 Comparison between optical surface images of Zn–Ni alloy coating (**a**) and Zn–Ni alloy composite elaborated with 10 g L^{-1} nano-TiO_2 (**b**)

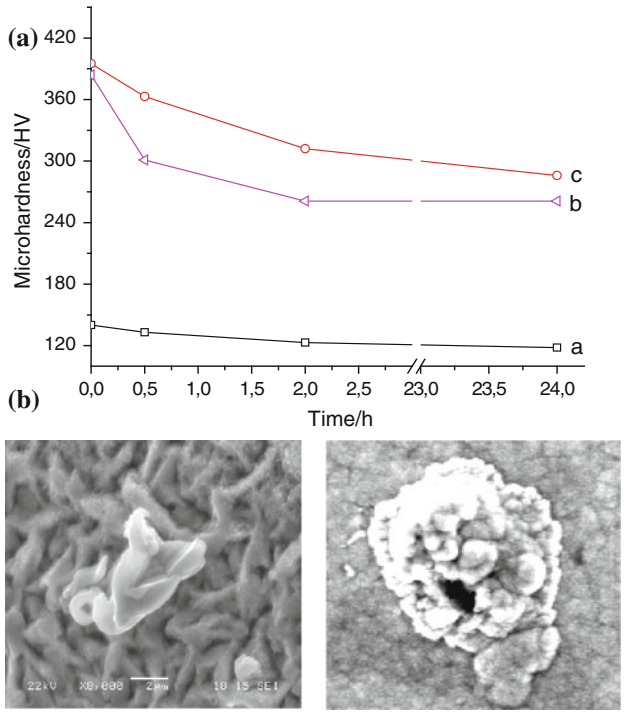

Fig. 4 **a** Variation of microhardness and SEM micrographs of Zn–Ni alloy coating (*a*) and Zn–Ni alloy composites elaborated with: (*b*) 5 g L^{-1} nano-TiO_2 and (*c*) 10 g L^{-1} nano-TiO_2, after heat treatment at 200 °C for 30 min, 2 h and 24 h. **b** SEM micrographs of surface areas of composites (*b*) and (*c*)

the hardness of composites decreased after 2 h. The reduced hardness could be attributed to surface oxidation phenomena or a rapid grain growth and a decrease of internal stresses as reported by Durairajan et al. [28]. SEM micrography of composite coating (Fig. 4b) proved a grain growth in some zones of the surface. Further heating for 24 h at 200 °C led to stable HV of composite deposits, these values were maintained higher than those of Zn–Ni alloy coating.

3.5 Corrosion resistance of the composite coatings immersed in 3 % NaCl solution

The variation of open-circuit potential with time in 3 % NaCl solution, shown in Fig. 5, was measured to obtain an insight to the corrosion protection behavior offered by Zn–Ni coatings. It could be seen that, there was not much fluctuation in the open-circuit potential behavior with time for all the samples, indicating the high protective action by these coatings. The corrosion potential (E_{corr}) shifted to positive values indicating a change in the content ratio in composite coatings and higher corrosion resistance compared with the Zn–Ni alloy coating.

EIS was used to evaluate the barrier properties of the coatings after 1 h of immersion in 3 % NaCl (pH 7.2) at 25 °C and to determine their polarization resistance. Figure 6a presented a comparison of Nyquist responses obtained for Zn–Ni elaborated without/and with nano-TiO_2 particles under the same quantities of electricity. The curves are composed of three overlapping semicircles, the

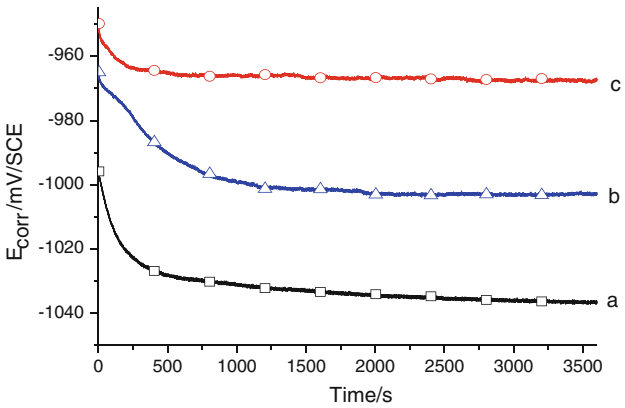

Fig. 5 Influence on the evolution of the corrosion potential of Zn–Ni alloy coating (*a*) and Zn–Ni alloy composites elaborated with: *b* 5 g L^{-1} nano-TiO_2 and *c* 10 g L^{-1} nano-TiO_2, immersed in solution 3 % NaCl (E_{corr} ± 6 mV/SCE)

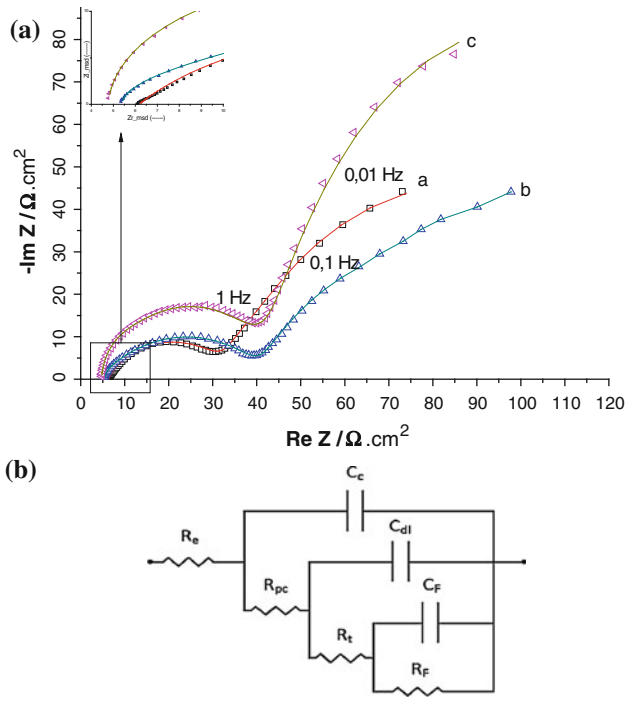

Fig. 6 **a** Nyquist responses (ground: experimental, *solid-line*: theoretical) of Zn–Ni alloy coating (*a*) and Zn–Ni alloy composites elaborated with: (*b*) 5 g L^{-1} nano-TiO_2 and (*c*) 10 g L^{-1} nano-TiO_2; $T = 25 \pm 2$ °C; immersion: 1 h in 3 % NaCl solution, **b** equivalent circuit used for Zn–Ni-coated steel to fit the impedance data

enlargement of the curves at high frequency showed the third semicircle.

The Nyquist-like diagram of the samples is characteristic of electrode process under kinetic and charge-transfer control. The polarization resistance R_p values could be approximately determined by fitting the Nyquist response to an equivalent circuit consisting of three RC components (Fig. 6b): the first time constant (R_{pc}, C_c) was attributed to the protective coating properties, (R_t, C_{dl}) an intermediate relaxation which R_t was the charge-transfer resistance of the corrosive process and C_{dl} was the double layer capacitance at the interface. This time constant was probably due to the heterogeneity of the film. The third time constant (R_F, C_F) in the low frequency part (1–10^{-2} Hz) could be attributed to the deposited corrosion products [29]. In all cases, the proposed model was in total agreement with the experimental data.

Nyquist diagrams showed that the impedance modulus of the samples rose with increasing the concentration of nano-TiO_2. The resistances (R_{pc}, R_t, and R_F) of Zn–Ni alloys, determined by fitting the parameters with CCE of Fig. 6b and summarized in the Table 3, was improved with increasing the concentration of nano-TiO_2 in the plating bath. It could be concluded that the addition of TiO_2 in the deposition process of Zn–Ni alloy on the surface substrate significantly increased the resistance to corrosion.

After the corrosion test, composition analyses by EDX indicated that the content of Zn in the deposit elaborated with 10 g L^{-1} nano-TiO_2 kept a higher value showing its extended life in corrosive media. It was proved also that Zn–Ni alloy composite, compared to the undoped alloy, covered more the surface of the substrate (Fe) and the chloride content, at the doped alloy surface was decreased significantly to 0.5 ± 0.2 %. Obviously, the TiO_2 played a major role for improving the corrosion protection in two mechanisms. First, these TiO_2 nano-particles acted as inert physical barriers to the initiation and development of defect corrosion, modifying the structure of Zn–Ni alloy and hence improving the corrosion resistance of the coating [30]. Second, dispersion of TiO_2 in the Zn–Ni alloy maybe resulted in formation of many corrosion micro cells in which the TiO_2 acted as cathode and the deposit acted as anode because of the standard potential of TiO_2 more positive than Zn–Ni. Such corrosion microcells facilitated the anode polarization [30].

After 48 h exposure to 3 % NaCl, the resistances (R_{pc}, R_t and R_F) and E_{corr} were increased with time (Fig. 7), denoting the improve of the corrosion protection.

4 Conclusion

The objective of this study was to investigate the effect of TiO_2 nano-particles on the properties of Zn–Ni matrix, putting emphasis on the correlation between composition and its effect on morphological and structure features under an extended region of electrodeposition conditions such as TiO_2 loading. With increasing amounts of TiO_2 nano-particles in the bath, the incorporation of nano-titania into Zn–Ni matrix, as well as the percentage of Ni, was found to increase. The concentration of the co-deposited particles

Table 3 Data obtained by electrochemical impedance spectroscopy and composition analyses by EDX of coatings immersed in 3 % NaCl solution for 1 h

Coating systems	Rpc ± 0.1 Ω cm^2	Q_f *10^{-5} F m^2 s^{α}	R_t ± 0.5 Ω cm^2	Q_f *10^{-5} F m^2 s^{α}	R_F ± 0.5 Ω cm^2	Q_f *10^{-5} F m^2 s^{α}	Composition analyses (±0.2 wt%)			
							Zn	Ni	Cl	Fe
Zn–Ni alloy coating	0.5	1	21	9	180	110.5	82	6	8.8	3.2
Zn–Ni composite (with 5 g L^{-1} TiO_2)	5.5	0.5	38	15.2	320	205	86	10.2	2.5	1.1
Zn–Ni composite (with 10 g L^{-1} TiO_2)	6	0.3	44	23.2	410	300.7	86.6	11.4	0.5	0.3

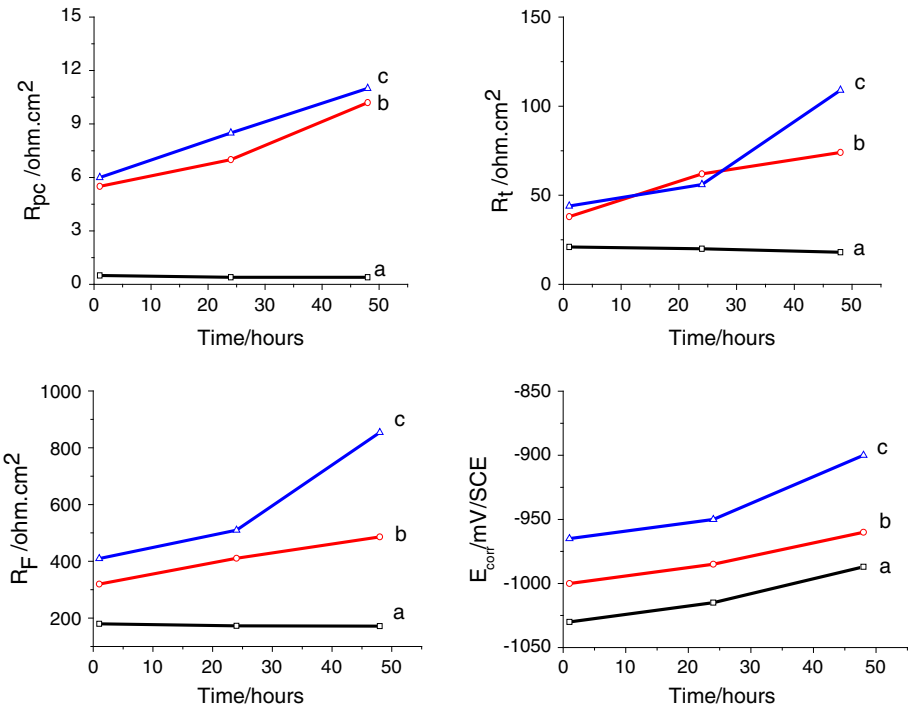

Fig. 7 Time dependence of coating resistance R_{pc}, charge-transfer resistance R_t, faradic resistance R_F and E_{corr} after 48 h for of Zn–Ni alloy coating (**a**) and Zn–Ni alloy composites elaborated with: (**b**) 5 g L^{-1} nano-TiO_2 and (**c**) 10 g L^{-1} nano-TiO_2; $T = 25 \pm 2$ °C, immersion: solution 3 % NaCl

affected the microhardness and the morphology of composite coatings. Heat treatment of all kinds of deposits at 200 °C resulted in crystallization of Zn–Ni matrix and their limited thermal stability. The tests of corrosion in 3 % NaCl solution showed an increase in corrosion resistance of composite coatings. The particles presence led to the Ni enrichment and so the improvement in the barrier properties of composite coatings.

Acknowledgments The authors would like to acknowledge the financial support provided by "Action Intégrée Franco-Tunisienne du Ministère des Affaires Etrangères et Européennes français et du Minstère de l'Enseignement Supérieur, de la Recherche Scientifique et de la Technologie tunisien".

References

1. Blejan D, Bogdan D, Pop M, Pop AV, Muresan LM (2011) Optoelectron Adv Mater 5(1):25–29
2. Kim S, Gislason JJ et al (2004) Chem Mater 16(12):2336–2343
3. Janeway PA (2003) Am Ceram Soc Bull 82(4):31–38
4. Losiewicz B, Stepien A, Gierlotka D, Bundiok A (1999) Thin Solid Films 349:43
5. de Tacconi NR, Boyles CA, Rajeshwar K (2006) Electrochem Soc 153:C449
6. Pavlatou EA, Stroumbouli M, Gyftou P, Spyrellis N (2006) Appl Electrochem 36:385–394
7. Gyftou P, Stroumbouli M, Pavlatou EA, Asimidis P, Spyrellis N (2005) Electrochim Acta 50:4544–4550
8. Schrestha NK, Masuko M, Saji T (2003) Wear 254:555
9. Deguchi T, Imai K, Matsui H, Iwasaki M, Tada H, Ito S (2001) J Mater Sci 36:4723
10. Jakob C, Erler F, Nutsch R, Steinhauser S, Wielage B, Zchunke A (2000) In: Proc. 15th Interfinish world exhibition, Garmisch-Partenkirchen, p 13–15 Sept
11. Lampke T, Leopold A, Dietrich D, Alisch G, Wielage B (2006) Surf Coat Technol 201:3510
12. Low CTJ, Willis RGA, Walsh FC (2006) Surf Coat Technol 201:371
13. Lampke T, Wielage B, Dietrich D, Leopold A (2006) Appl Surf Sci 253:2399
14. Erler F, Jakob C, Romanus H, Lampke T (2003) Electrochim Acta 48:3063
15. Guglielmi N (1972) Electrochem Soc 119–8:1009
16. Hammami O, Dhouibi L, Triki E (2009) Surf Coat Technol 203:2863–2870
17. Klug HP, Alexander LE (eds) (1954) X-ray diffraction procedures for polycrystalline and amorphous materials. Chapman and Hall, London
18. Hovestad A, Jansen LJJ (2005) In: Conway BE et al (eds) Modern aspects of electrochemistry, vol 38, chap 6. Kluwer Academic/Plenum Publishers, New York, p 475
19. Azizi M, Schneider W, Plieth W (2005) Solid State Electrochem Soc 9:429
20. Hiemenz PC (ed) (1986) Principles of colloid and surface chemistry. Marcel Dekker, New York
21. Banovic SW, Barmak K, Marder AR (1999) J Mater Sci 34:3203
22. Chen ES, Lakshminarayanan GR, Sautter FK (1971) Met Trans 942:937
23. Li J, Sun Y, Sun X, Qiao J (2005) Surf Coat Technol 192:331
24. Brenner A (ed) (1963) Electrodeposition of alloys: principles and practice, vol 2. Academic Press, New York, p 194
25. Alfantazi A, El-Sherik AM, Erb U (1994) Scripta Metall Mater 30:1245–1250
26. Portinha A, Teixeire V et al (2005) Surf Coat Technol 200:765
27. Gachard E, Belloni J, Subramanian MA (1996) J Mater Chem 6:867
28. Apachitei I, Tichelaar FD, Duszczyk J, Katgerman L (2002) Surf Coat Technol 149:263
29. Durairajan A, Haran BS, White RE, Popov BN (2000) Electrochem Soc 147(5):1781–1786
30. Chen XH, Chen CS, Xiao HN, Cheng FQ, Zhang G, Yi GJ (2005) Surf Coat Technol 191:351